Proceedings of the ASME 2011 International Mechanical Engineering Congress & Exposition
IMECE2011
November 11-17, 2011, Denver, Colorado, USA

IMECE2011-65878

3-D INVERSE HEAT TRANSFER IN A COMPOSITE TARGET SUBJECT TO HIGH-ENERGY LASER IRRADIATION

Jianhua Zhou, Yuwen Zhang[1,2,3], J.K. Chen[2,3] and Z.C. Feng[2,3]
Department of Mechanical and Aerospace Engineering
University of Missouri
Columbia MO 65211, USA

ABSTRACT

A new numerical model is developed to simulate the 3-D inverse heat transfer in a composite target with pyrolysis and outgassing effects. The gas flow channel size and gas addition velocity are determined by the rate equation of decomposition chemical reaction. The thermophysical properties of the composite considered are temperature-dependent. A nonlinear conjugate gradient method (CGM) is applied to solve the inverse heat conduction problem for high-energy laser-irradiated composite targets. It is shown that the front-surface temperature can be recovered with satisfactory accuracy based on the temperature/heat flux measurements on the back surface and the temperature measurement at an interior plane.

INTRODUCTION

Fiber-reinforced composite materials have gained wide applications in military and industry [1]. Due to unique properties such as monochromaticity and directionality, high energy laser (HEL) beams are now employed as a weapon to defeat adversary military targets. To evaluate target damage, a direct heat transfer model is required to simulate temperature transients inside a laser-irradiated composite target with known initial and boundary conditions. Currently, many theoretical models are available for this purpose. For example, Reed and Rice [2] developed a rate dependent pyrolysis model to characterize the heat transfer in decomposing material. Chen et al. [3] used a modified Crank-Nicholson finite difference scheme to model the heat transfer process in laser-irradiated composites. Zhou et al. [4] developed a 1-D nonequilibrium thermal model to predict the through-thickness transient temperature variation in a composite slab subjected to intensive laser heating. The cooling effect arising from pyrolysis reaction was simulated using a two dimensional gas flow model with an assumed gas addition velocity and the microchannel shape [5].

For a solid subjected to intensive laser beam heating, the heated (front) surface is either inaccessible or too hot so that it is not suited for attaching a sensor to measure temperature response [6]. Under this circumstance, some researchers propose to determine the heated surface temperature indirectly by solving an inverse heat conduction (IHC) problem [7, 8] based on the transient temperature and/or heat flux measured at the back surface. Although IHC problems have been extensively studied for different applications in the past (e.g., [9-12]), little work has been done for composite materials subjected to high energy laser heating. Though Aviles-Ramos et al. [13] developed an exact solution for the IHC in a two-layer composite material, the pyrolysis effect was not considered in their model. Recently, the authors proposed a low-error IHC algorithm to reconstruct the front-surface heating condition of a 1-D composite slab with pyrolysis effect based on the back-surface measurement information [14]. The pyrolysis outgassing model was from Ref. [4], in which the gas addition velocity and the microchannel size were assumed.

In this study, a new 3-D IHC model is formulated to recover transient heat flux and temperature at the heated surface of composite targets heated by a high energy laser. The target is assumed to be of rectangular geometry. The pyrolysis process is characterized based on a new gas flow model. The gas flow channel size and gas addition velocity are determined by the rate equation of pyrolysis chemical reaction. The nonlinear 3-D IHC problems are solved using a nonlinear conjugate gradient method (CGM) based on three groups of measurement data including temperature and heat flux at back surface as well as

[1] Corresponding author. zhangyu@missouri.edu
[2] Fellow ASME
[3] Professor

Copyright © 2011 by ASME

the temperature at an interior plane. Demonstrative simulations are performed and results are presented.

NOMENCLATURE

A_c	cross-section area of the gas channel, m
$A_c^{'}$	new cross-section area of the gas channel after conversion (Eq.(13)), m
c_{pg}	specific heat of gas at constant pressure, J/(kg·K)
C	volume specific heat of solid constituent of composite, J/(m^3·K)
$D(x)$	inner diameter of gas flow channel, m
f	frequency of periodic laser heat flux on the front surface, Hz
f_r	friction coefficient
$G(x,y,z,t)$	heat source due to convective heat exchange between pyrolysis gas and solid part, W/m^3
h_{gas}	convection heat transfer coefficient, W/(m^2·K)
ΔH	chemical reaction heat, J/kg
k	thermal conductivity of solid constituent, W/(m·K)
L, M, N	object lengths in the x, y, and z directions, respectively, m
$\dot{m}$	mass flux of gas addition, kg/(m^2•s)
M_a	Mach number
p	pressure, Pa
q_{laser}	periodic laser heating flux on the front surface, W/m^2
q_0^*	maximum heat flux at the laser Gaussian beam center, W/m^2
$q_1(y,z,t)$	absorbed heat flux on front surface, W/m^2
δq	heat addition per unit mass of gas, J/kg
$Q(x,y,z,t)$	heat generation arising from thermal decomposition, W/m^3
r	radius measured from the laser spot center, m
R_c	outer radii of the gas flow channel, m
$R_c^{'}$	new outer radii of the gas flow channel after conversion, m
R_f	outer radii of fiber, m
S	objective function
t	time, s
t_f	final time, s
t_{pyro}	pyrolysis onset time, s
T	temperature, K
T_0	initial temperature, K
$T_1(y,z,t)$	front-surface temperature, K
T_{go}	stagnation temperature, K
V	gas flow velocity along the x-direction, m/s
w	1/e radius of Gaussian laser beam, m
x, y, z	coordinate variables, m
$Y_{qLexact}(y,z,t)$	measurement heat flux without errors on the back surface, W/m^2
$Y_{qL}(y,z,t)$	measurement heat flux on the back surface, W/m^2
$Y_{TL}(y,z,t)$	measurement temperature on the back surface, K

Greek symbols

α	volume fraction of decomposed material
δ_q	standard deviation of the heat flux measurement, W/m^2
ρ	density, kg/m^3
ω	random variable having a normal distribution with zero mean and unitary standard deviation

Subscripts

0	initial
f	final
g	gas
q	heat flux
T	temperature

INVERSE HEAT CONDUCTION PROBLEM

3-D inverse heat conduction model

Consider a 3-D composite object with dimensions L×M×N as shown in Fig. 1. The Cartesian coordinate system O-xyz is set with the origin locating at a corner of the object. Initially, the object is at a uniform temperature T_0 and then is subjected to a high intensity, Gaussian laser beam q_{laser} with a 1/e radius w centered on the front surface (x = 0) from t = 0$^+$. Before the pyrolysis occurs, only pure conduction takes place in the composite. After the temperature reaches to a threshold, the

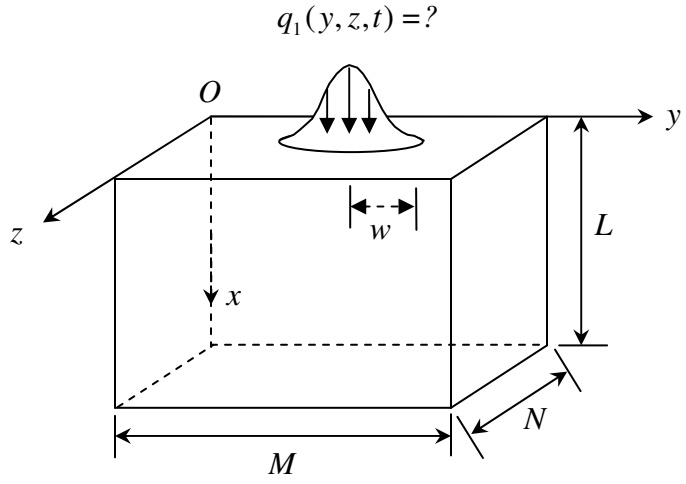

Figure 1 Physical model

Copyright © 2011 by ASME

composite material undergoes chemical decomposition. Meanwhile, the decomposing process gives off gaseous byproducts that flow outward from the pyrolysis zone to the heated surface. Since the pyrolysis occurs only in a confined region inside the material, this pyrolysis outgassing process is approximated as a 1-D compressible gas flow along the *x*-direction.

The direct problem in the 3-D target can be expressed as follows:

$$C(T)\frac{\partial T}{\partial t}=\frac{\partial}{\partial x}[k(T)\frac{\partial T}{\partial x}]+\frac{\partial}{\partial y}[k(T)\frac{\partial T}{\partial y}]+\frac{\partial}{\partial z}[k(T)\frac{\partial T}{\partial z}]+Q(x,y,z,t)+G(x,y,z,t)$$
$$\text{for } 0<x<L,\ 0<y<M,\ 0<z<N,\ t>0 \quad (1)$$

$$T=T_0 \quad \text{for} \quad 0\le x\le L,\ 0\le y\le M,\ 0\le z\le N,\quad t=0 \quad (2)$$

$$-k(T)\frac{\partial T}{\partial x}=q_1(y,z,t) \quad \text{for} \quad x=0,\quad t>0 \quad (3)$$

$$T=2\cdot Y_{TL}(y,z,t)-T_g \quad \text{for} \quad x=L,\quad t>0 \quad (4)$$

$$-k(T)\frac{\partial T}{\partial y}=0 \quad \text{for} \quad y=0,\ M;\ t>0 \quad (5)$$

$$-k(T)\frac{\partial T}{\partial z}=0 \quad \text{for} \quad z=0,\ N;\quad t>0 \quad (6)$$

where T is the temperature of the solid part; $Q(x,y,z,t)$ is the heat generation arising from the thermal decomposition; $G(x,y,z,t)$ is the heat source due to the convective heat exchange between the pyrolysis gas and the solid part; $q_1(y,z,t)$ is the net heat flux at the front surface; $Y_{TL}(y,z,t)$ is the measurement temperature on the back surface ($x = L$), which is the mean value of fiber temperature and matrix temperature; T_g is the temperature of the pyrolysis gas; k is the thermal conductivity which is temperature-dependent and changes as pyrolysis progresses [3]; C is the volume specific heat, calculated by combining the corresponding values of the fibers and matrix, depending on the fraction of the decomposed material [4].

It must be pointed out that the term "solid part" in this paper is used to describe the material part in solid state which is a combination of fiber and matrix when the pyrolysis is in progress. However, it refers to the fiber only after the pyrolysis is completed.

Eq. (4) is written based on the premise that the measurement temperature at an interior location is the average of the local solid and gas temperatures.

The pyrolysis is a rate-dependent process and the generated heat source term $Q(x,y,z,t)$ in Eq. (1) is obtained by

$$Q(x,y,z,t)=-\frac{\rho\Delta H}{1-\alpha}\cdot\frac{d\alpha}{dt} \quad (7)$$

where ρ is density of solid part; ΔH is the chemical reaction heat; α is the volume fraction of the decomposed material, which is evaluated based on the rate equation:

$$\frac{d\alpha}{dt}=A(1-\alpha)^{M_o}e^{B/T} \quad (8)$$

where A is the frequency factor, B is activation energy, and M_o is the order of the decomposition reaction.

The convective heat exchange term in Eq.(1), $G(x,y,z,t)$, is expressed as:

$$G(x,y,z,t)=\frac{h_{gas}(T_g-T)}{R_f^2(1-\alpha)/2R_c}H(t-t_{pyro}) \quad (9)$$

where h_{gas} is the convection heat transfer coefficient between the gaseous byproducts and the solid part of the composite, which is computed based on 1-D compressible gas flow simulation; R_f and R_c are the outer radii of the fiber and gas flow channel, respectively; t_{pyro} is pyrolysis onset time; $H(t-t_{pyro})$ is Heaviside step function, which is zero before pyrolysis $(t<t_{pyro})$ and one after pyrolysis $(t>t_{pyro})$.

In the direct problem described above, the front-surface heat flux $q_1(y,z,t)$ and the back surface temperature $Y_{TL}(y,z,t)$ are considered to be known. The objective of the direct problem is to determine the transient temperature and heat flux distribution in the composite target.

The inverse problem associated with the above-defined direct problem can be stated as follows. The heat flux $q_1(y,z,t)$ at the front surface ($x = 0$) is unknown and needs to be recovered. The temperature measurement on the back surface, $Y_{TL}(y,z,t)$, is used as the boundary condition at $x = L$. The heat flux measurements on the back surface, $Y_{qL}(y,z,t)$, and temperature measurements $Y_{T1}(y,z,t)$ at the interior plane of $x = x_1$ are utilized as extra information required to recover the front surface heat flux. The front surface temperature is calculated as a by-product according to the temperature-heat flux relation defined by the classical Fourier's law.

The conjugate gradient method (CGM) [8] is applied to solve the IHC problem. The inverse solution is obtained by minimizing the following functional (referred to as *objective function*):

$$S[q_1(t)]=\int_0^{t_f}\{Y_{qL}(t)-q[L,t;q_1(t)]\}^2dt+\int_0^{t_f}\{Y_{T1}(t)-T[x_1,t;q_1(t)]\}^2dt \quad (10)$$

where t_f is the final simulation time, $q[L,t;q_1(t)]$ is the estimated heat flux at the back surface, and $T[x_1,t;q_1(t)]$ is the estimated average temperature at the interior position x_1.

The CGM mathematical formulation for the nonlinear inverse problems involving temperature-dependent thermal properties is similar to that in Ref. [14]. It is not described here for brevity.

1-D compressible gas flow

It is assumed that the gas flow produced by pyrolysis reaction is one-dimensional along the *x*-direction. The physical

Copyright © 2011 by ASME

model of the 1-D gas flow is depicted in Figure 2. The black regions represent fibers, the gray regions denote matrix, and the white regions represent the gas flow channels. Each gas flow channel, together with its surrounding material, constitutes an element as the dash-line box shown in Fig. 2.

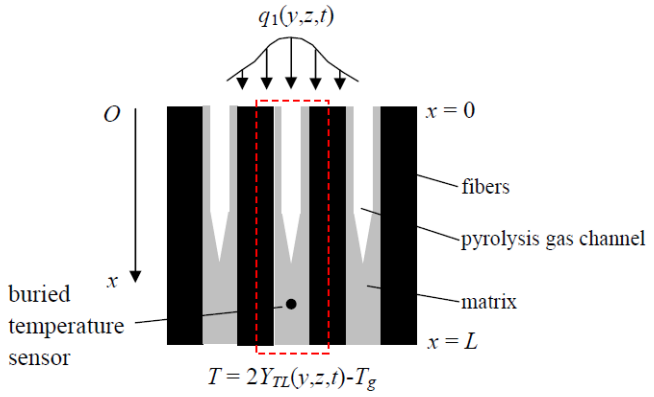

Figure 2 Physical model of 1-D gas flow channels.

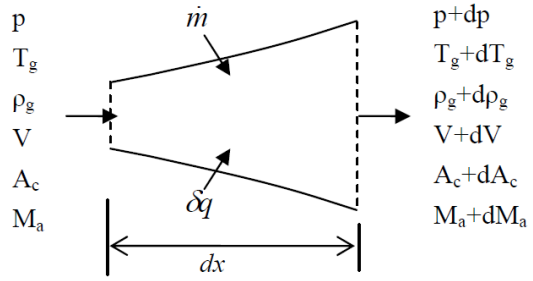

(a)

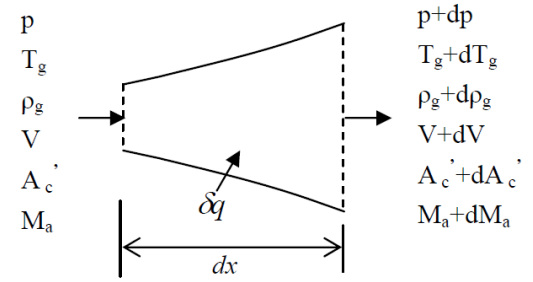

(b)

Figure 3 The 1-D gas flow with mass addition in (a) is converted to a 1-D gas flow without mass addition but with extra area change in (b).

The 1-D gas flow in the gas channel (white region in Fig. 2) is a compressible gas flow problem with area change, friction, heat and mass addition. It is intractable since it is involved with many complicated factors, among which the mass addition is the trickiest one. Solution for such a gas flow problem has not been reported in literatures. To overcome this difficulty, the 1-D gas flow with mass addition will be converted to a 1-D gas flow without mass addition but with extra area change [15, 16]. This can be explained with the aid of Fig. 3.

Take an infinitesimal section dx for consideration. The parameters appearing in Fig. 3 are as follows: x is the coordinate variable, p pressure, T_g temperature, ρ_g density, V gas flow velocity along the x-direction, A_c cross-section area of the gas channel, M_a Mach number, $\dot{m}$ mass flux of gas addition (units: kg/(m^2•s)), and δq the heat addition per unit mass of gas (units: J/kg).

The continuity equation for the 1-D gas flow with mass addition in Fig. 3 (a) can be written as:

$$\frac{d(\rho_g V)}{dx} = -\frac{\rho_g V}{A_c}\frac{dA_c}{dx} + \frac{\dot{m}\cdot\pi D(x)}{A_c} \tag{11}$$

where $D(x)$ is the inner diameter of the gas flow channel. For the gas flow without mass addition in Fig. 3 (b), the continuity equation is given by:

$$\frac{d(\rho_g V)}{dx} = -\frac{\rho_g V}{A_c'}\frac{dA_c'}{dx} \tag{12}$$

By comparing Eqs. (11) and (12), one can see that the gas flow with mass addition in Fig. 3(a) can be converted to a gas flow without mass addition shown in Fig. 3(b). The new cross-section area A_c' can be obtained by equating Eqs. (10) and (11):

$$\frac{dA_c'}{A_c'} = \frac{dA_c}{A_c} - \frac{\dot{m}\cdot\pi D(x)dx}{\rho_g A_c V} \tag{13}$$

where A_c' is the new cross-section area after conversion; A_c is the cross-section area before conversion:

$$A_c = \pi R_c^2 = \alpha\cdot\pi R_f^2 \tag{14}$$

The mass flux $\dot{m}$ of gas addition in Eq. (1) is computed based on a 3-D porous structure using the local volume averaging method [17]:

$$\dot{m} = \frac{1}{2}\rho\frac{R_f^2}{R_c}\frac{d\alpha}{dt} \tag{15}$$

Based on the conversion described above, the 1-D compressible gas flow in a composite material can be simulated by the gas flow without mass addition shown in Fig. 3(b). We can then summarize the continuity, momentum and energy conservation equations for the gas flow problem in Fig. 3(b) as follows [16]:

$$\frac{d\rho_g}{\rho_g} + \frac{dA_c'}{A_c'} + \frac{dV}{V} = 0 \tag{16}$$

$$dp + \frac{1}{2}\rho_g V^2\frac{f_r dx}{D} + \rho_g V dV = 0 \tag{17}$$

$$\delta q = c_{pg} dT_{go} \tag{18}$$

where f_r is the friction coefficient, which is defined as $f_r = 4\tau_f/(1/2\rho V^2)$ with τ_f being the shear stress due to wall friction; c_{pg} is the mass specific heat of gas at constant pressure;

Copyright © 2011 by ASME

T_{go} is stagnation temperature (or referred to as *total temperature*), which is related to true temperature T_g by:

$$\frac{T_{go}}{T_g} = 1 + \frac{\gamma - 1}{2} M^2 \tag{19}$$

where $\gamma = c_{pg} / c_{vg}$ is the ratio of specific heat.

Combining the governing equations (16)~(18), the ideal gas law

$$\frac{dp}{p} - \frac{d\rho_g}{\rho_g} - \frac{dT_g}{T_g} = 0 \tag{20}$$

and the Mach number equation

$$\frac{dT_g}{T_g} + \frac{dM_a^2}{M_a^2} - \frac{dV^2}{V^2} = 0 \tag{21}$$

one can reach a final equation which is utilized to calculate the Mach number as a function of x:

$$\frac{dM_a}{dx} = \frac{M_a}{1 - M_a^2} \left[-\frac{1 + \frac{\gamma - 1}{2} M_a^2}{A_c^{'}} \frac{dA_c^{'}}{dx} + \frac{\gamma}{2} \frac{f_r}{D} M_a^2 \left(1 + \frac{\gamma - 1}{2} M_a^2\right) + \frac{1 + \gamma M_a^2}{2 c_{pg} T_g} \frac{\delta q}{dx} \right] \tag{22}$$

After the gas flow velocity is determined by Eq. (22), the convective heat exchange between the pyrolyzed gas and the surrounding composite materials can be evaluated by the Reynolds's analogy approach, in which the convective heat transfer coefficient can be calculated as [16]:

$$h_{gas} = \frac{1}{8} \rho_g V c_{pg} f_r \tag{23}$$

According to Eq. (18), the heat exchange between gas and the solid wall is calculated as:

$$\delta q = c_{pg} dT_{go} = h_{gas} (T - T_{g0}) 2\pi R_c^{'} dx \tag{24}$$

where $R_c^{'}$ is the radius of the gas flow channel after conversion. Substitution of Eq. (23) into Eq. (24) results in:

$$\frac{dT_{g0}}{T - T_{g0}} = \frac{f_r}{4 R_c^{'}} dx \tag{25}$$

Equation (25) is used to calculate the gas stagnation temperature T_{g0}, which in turn, is applied to compute gas true temperature T_g using Eq. (19). Then, the convective heat exchange term $G(y, z, t)$ can be estimated from Eq. (9).

SOLUTION PROCEDURE

As seen from the description in the previous section, the heat conduction in the solid constituent and the pyrolysis gas flow is coupled to each other. An iterative procedure is devised to solve this problem, which is summarized as follows for each time step:

(1) Use $Q(y, z, t)$ and $G(y, z, t)$ at the previous time step as the initial guess for the current time step. Since the heat transfer mechanism in composite is pure heat conduction at early stage, it is reasonable to assume that the heat generation term, $Q(y, z, t)$, and convective heat exchange term, $G(y, z, t)$, are zero for the first time step.

(2) Solve the heat conduction Eqs. (1)~(6) in the solid constituent.

(3) Calculate the volume fraction of the decomposed material, α, using Eq. (8) and mass flux $\dot{m}$ using Eq. (15).

(4) Compute new size $A_c^{'}$ of the gas channel using Eq. (13).

(5) Calculate the gas stagnation temperature T_{g0} and the gas temperature T_g using Eqs. (25) and (19), respectively.

(6) Update the heat generation term, $Q(y, z, t)$, and the convective heat exchange term, $G(y, z, t)$, using Eqs. (7) and (9), respectively.

(7) Calculate the relative difference of the solid temperatures at the current and previous iteration. If the relative difference is less than a prespecified small value, e.g. 0.001, stop the iterative procedure and proceed to the next time step; otherwise, go back to step 2 and continue the iterative process.

RESULTS AND DISCUSSION

Generation of simulated measurement data

Instead of conducting actual experiment, the measurement data of temperature and heat flux are generated numerically by solving a direct problem with radiation and convection boundary conditions. Here, the "direct problem" is not exactly the same as that defined in Eqs. (1)~(6). Only after Eq.(3) and Eq.(4) are replaced by radiation and convection boundary conditions, Eqs.(1)~(6) can be used for the generation of simulated measurement data. To account for the measurement error, one extra term is added to the simulated heat flux measurement data, $Y_{qLexact}(y, z, t)$:

$$Y_{qL}(y, z, t) = Y_{qLexact}(y, z, t) + \omega \delta_q \tag{26}$$

where $Y_{qLexact}(y, z, t)$ is the simulated measurement data from the direct problem; δ_q is the standard deviation of the heat flux measurement and is set as a percentage of the highest heat flux value at the back surface; ω is a Gaussian random variable with standard deviation of unity. It is assumed that the temperature readings at back surface and interior locations contain no errors since temperature can be measured with much less uncertainty compared to the heat flux [18].

Simulation parameters

A carbon fiber/epoxy composite is taken as the demonstrative material. The dimension of the 3-D object is 3.0 × 68.4 × 68.4 mm. The laser heating flux at the front surface is assumed to be Gaussian in space and sinusoidal in time:

$$q_{laser}(y, z, t) = q_0^{''} \cdot \exp\{-(y^2 + z^2) / w^2\} \cdot (1 + \sin(2\pi f t) \tag{27}$$

where $q_0^{''}$ is the heat flux at the laser beam center (averaged over one period) ; f is the frequency of the laser heating flux. In this study, the following simulation parameters are used unless otherwise specified: $q_0^{''}$ = 150 W/cm^2, f = 3.0 Hz, w = 7.6 mm,

Copyright © 2011 by ASME

and the measurement random error in back-surface heat flux $\delta_q = 5\% \cdot [Y_{qLexact}(t)]_{\max}$.

The 3-D finite difference mesh used is 53×13×13. The dense mesh in x direction (53) ensures the exact capturing of the pyrolysis progress. To measure both temperature and heat flux at the back surface, a fully-populated temperature and heat flux sensor array should be attached to the surface. Another fully-populated temperature sensor array should be inserted to an interior plane at $x = x_1$ to measure the temperature. In this study, the interior plane location is at x_1 = 0.2 mm. Our simulation shows that for low thermal conductivity materials, interior temperature measurement data are necessary to accurately recover the front-surface heating condition. The lower the thermal conductivity is, the closer the location x_1 should be moved toward the front surface. The temperatures and heat flux obtained from the direct analysis will be used as the measurement data for IHC analysis.

The pyrolysis gas is approximated as CO_2 whose thermal properties can be found in standard thermophysics textbook. The density and specific heat of the carbon fiber are 1603 kg/m^3 and 1267 J/(kg·K), respectively. The density and specific heat of the epoxy matrix are 1100 kg/m^3 and 600 J/(kg·K), respectively. The thermal conductivity of carbon/epoxy composite is considered temperature-dependent, which is shown in Figure 4.

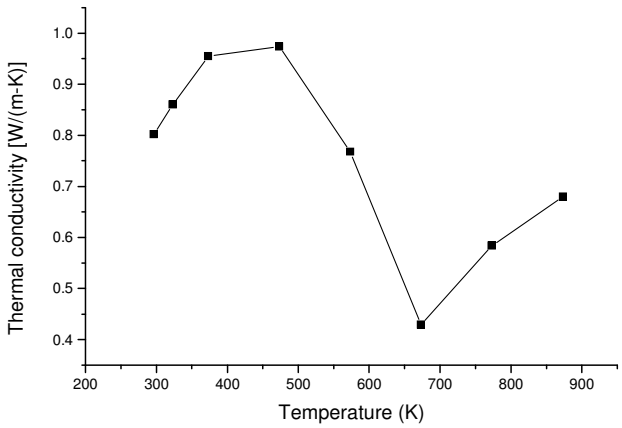

Figure 4 Thermal conductivity of carbon/epoxy composite [3].

Results of direct problem

Figure 5 shows the temperature transients at the laser spot center on the front surface of the composite heated by a laser beam with $q_0^{"}$ = 150 W/cm^2. For comparison, the result obtained by a pure heat conduction model, which does not consider the pyrolysis gas flow effect, is also shown. It can be seen that the two curves in Fig. 5 are identical before the onset of pyrolysis, at about 0.7 s. After that, the two curves diverge from each other. This is because pyrolysis reaction begins and the decomposing process gives off gaseous byproducts that flow outward from the pyrolysis zone to the front surface. The outgassing flow has a cooling effect on the composite bulk heated by laser irradiation, as evidenced by the observation in Fig. 5 that the Curve 2 is below Curve 1 after t = 0.7 s (Fig. 5(a)) and the difference between Curve 2 and Curve 1 is negative (Fig. 5(b)). In addition, as seen in Fig. 5(b), the difference between the results with and without pyrolysis is also fluctuates after the pyrolysis begins. The difference becomes smaller and smaller as time proceeds, indicating that the convective heat transfer effect due to pyrolysis becomes weaker with time.

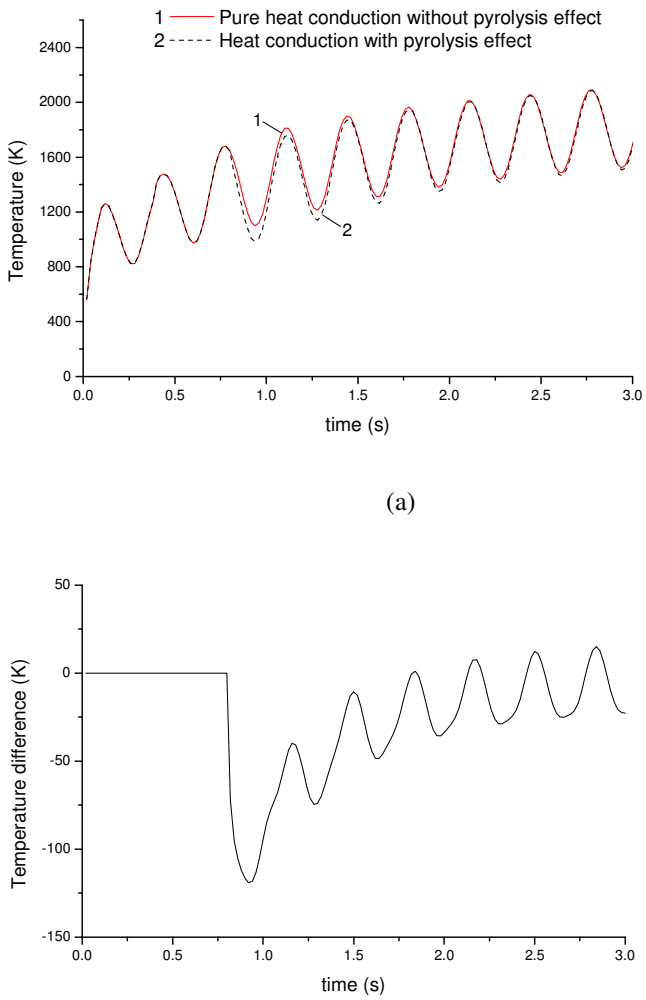

Figure 5 Temperature transients at the laser spot center on the front surface for $q_0^{"}$ = 150 W/cm^2. (a) comparison of the results with and without pyrolysis effect. Curve 1: Pure heat conduction without pyrolysis effect. Curve 2: Heat conduction with pyrolysis effect. (b) difference between the results with and without pyrolysis effect (Curve 2 minus Curve 1).

Copyright © 2011 by ASME

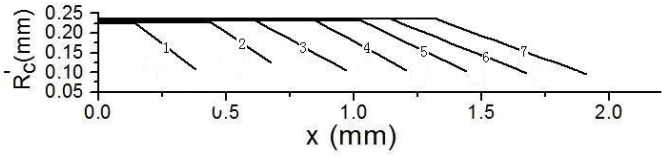

Figure 6 Temporal evolvement of the gas channel shape. Label is time (s).

Figure 6 shows the temporal evolvement of the gas channel shape. It appears that the gas channel shape can be divided to two sections. One section is flat (e.g., x = 0~1.3 mm for Curve 7), which corresponds to the status in which the decomposed α reaches its maximum value $\alpha_{\max}$. The other section is the gradually converging section (e.g., x = 1.3 ~ 1.9 mm for Curve 7), which corresponds to the status in which $\alpha < \alpha_{\max}$. It can be clearly seen that the pyrolysis front advances toward deeper location of the composite as time elapses.

Figure 7 presents the distribution of the convective heat transfer coefficient h_{gas} along the x direction. The convective heat transfer due to pyrolysis at t = 2s is the strongest. It is also observed that the distribution of h_{gas} for all times can be divided to two sections. The horizontal sections of the curves correspond to $\alpha = \alpha_{\max}$, which means that the pyrolysis is completed in this region. The gradually-increasing sections of the curves correspond to $\alpha < \alpha_{\max}$, in which section drastic pyrolysis reaction is occurring. Besides, it is seen from Fig. 7 that, after t = 2s, the convection heat coefficient h_{gas} decreases with time at any particular x. This is because that as the chemical reaction proceeds, the amount of the pyrolyzed gas becomes less.

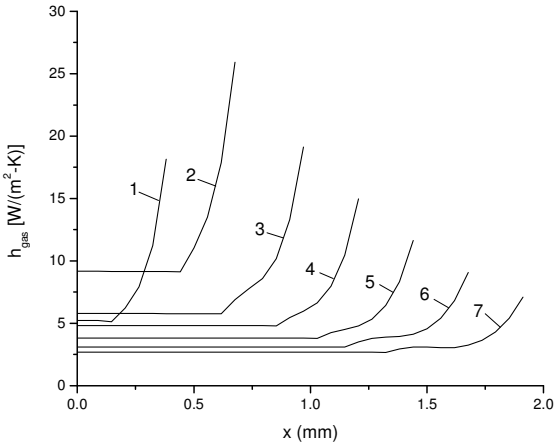

Figure 7 Distribution of the convective heat transfer coefficient along the x direction. Label is time (s).

Results of inverse problems

Figure 8 shows the recovered temperatures at the laser spot and at the radius of 13.4 mm (the 1/e radius w = 7.6 mm). The location of 13.4mm is chosen in a random way for illustrative purpose. The "exact solutions" shown in Fig. 8 are obtained from the solution of the direct problem with the radiation boundary conditions. As can be seen in Fig. 8, the temperatures can be well recovered from the IHC analysis. As can be seen from the difference between exact solution and inverse solution (Fig. 8(b)), the largest error seems occurring at the most drastic moment of pyrolysis (at about 0.8s). This is due to the extreme nonlinearity caused by the compressible gas flow. The RMS difference between the exact and inverse solutions is calculated over the entire front surface and entire simulation time length, which is 3.36 K for this case.

Figure 9 compares the 2-D distributions of the recovered temperatures at the front surface at the time of 4.0 s. On this scale, the temperatures over the entire front surface appear identical

Figure 10 plots the contour distributions of the errors in the recovered temperatures from 1s to 6s. As shown in Figs. 10 (a)-(f), the errors of the inverse solutions at t = 1s is the highest. The errors at other times are quite small, less than 2 K. The location of the maximum error is not fixed, varying from time to time. However, the distributions of the numerical errors seem to be symmetric with regard to the laser spot center.

Figure 11 presents the simulation results when $q_0^{"}$ is increased to 300 W/cm^2. The temperatures at the laser spot center on the front surface are shown in Fig. 11 (a). The cooling effect can be clearly seen and the pyrolysis onset time is about 0.5 s, which is earlier than that (0.7 s) of the case $q_0^{"}$ = 150 W/cm^2. The most drastic convective cooling effect is present from 0.5 s - 0.7 s, shorter than that for the case of $q_0^{"}$ = 150 W/cm^2 (from 0.7 s to 2.2 s).

Fig. 11 (b) shows the convective coefficient distribution along the x direction. Comparing the results in Fig. 11 (b) with Fig. 7, we can see that the convective coefficients at early stage (e.g., t = 1 s and 2 s) increase with the increase of the laser heating flux $q_0^{"}$. However, as time proceeds, the convective coefficients becomes almost the same for the two cases (after t = 3 s). This indicates that the elevation of the laser heating flux can only have significant influence on the early stage of the pyrolysis. In addition, we see that the lengths of the horizontal section at a particular time moment are different for the two cases shown in Fig. 11 (b) and Fig. 7. The length of the horizontal section for the case $q_0^{"}$ = 300 W/cm^2 is about two times longer than that for $q_0^{"}$ = 150 W/cm^2. For example, the length of the horizontal section at t = 3 s (curve 3) in Fig. 6 is about 0.6 mm, while it is about 1.0 mm in Fig. 11 (b). This indicates that increasing the laser heating flux can cause pyrolysis at deeper depths.

Copyright © 2011 by ASME

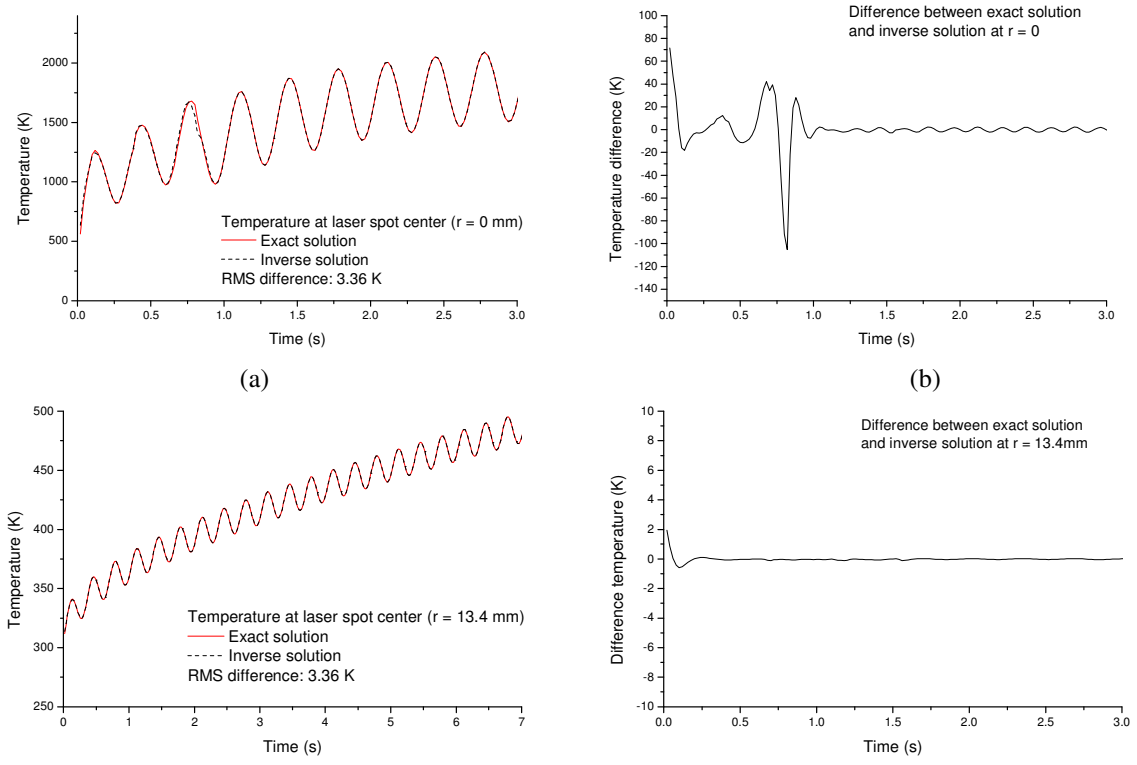

Figure 8 Recovered temperatures on the front surface (f = 3Hz): (a) comparison of exact solution and inverse solution at the laser spot center; (b) difference between the exact solution and inverse solution at the laser spot center (inverse solution minus exact solution); (c) comparison of exact solution and inverse solution at the radius of 13.4 mm; (d) difference between the exact solution and inverse solution at the radius of 13.4 mm (inverse solution minus exact solution).

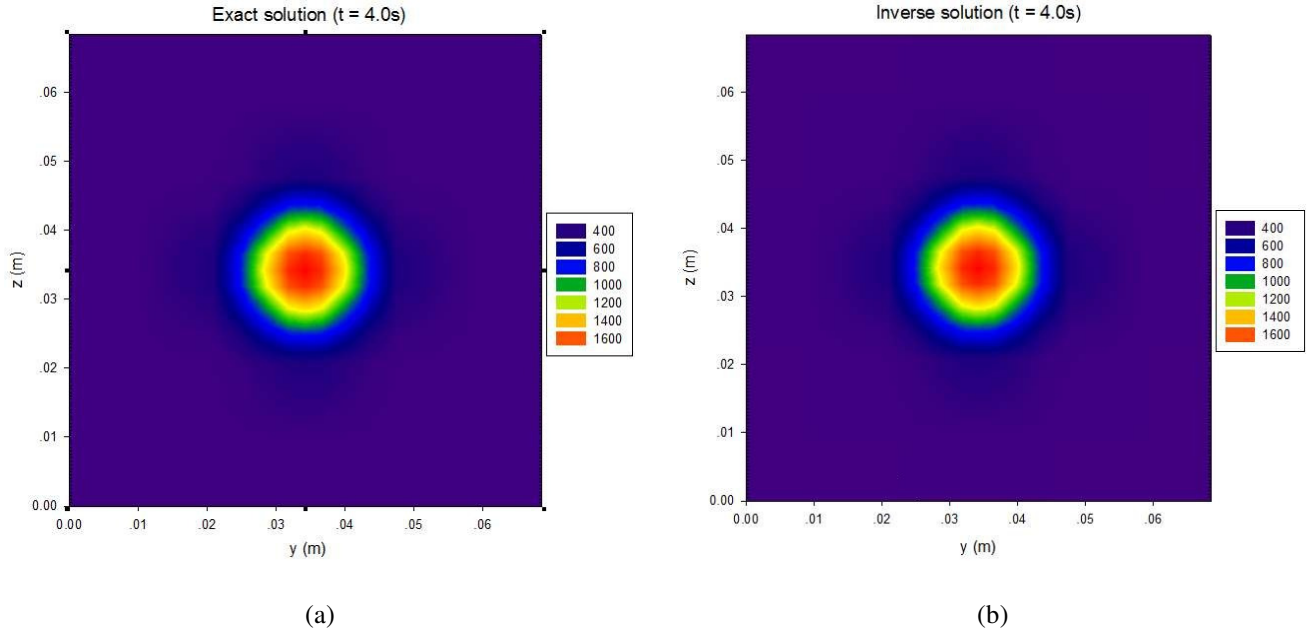

Figure 9 2-D contour distributions of the recovered temperatures at the front surface at the time of 4 s: (a) Exact temperature distribution; (b) Recovered temperature distribution.

Copyright © 2011 by ASME

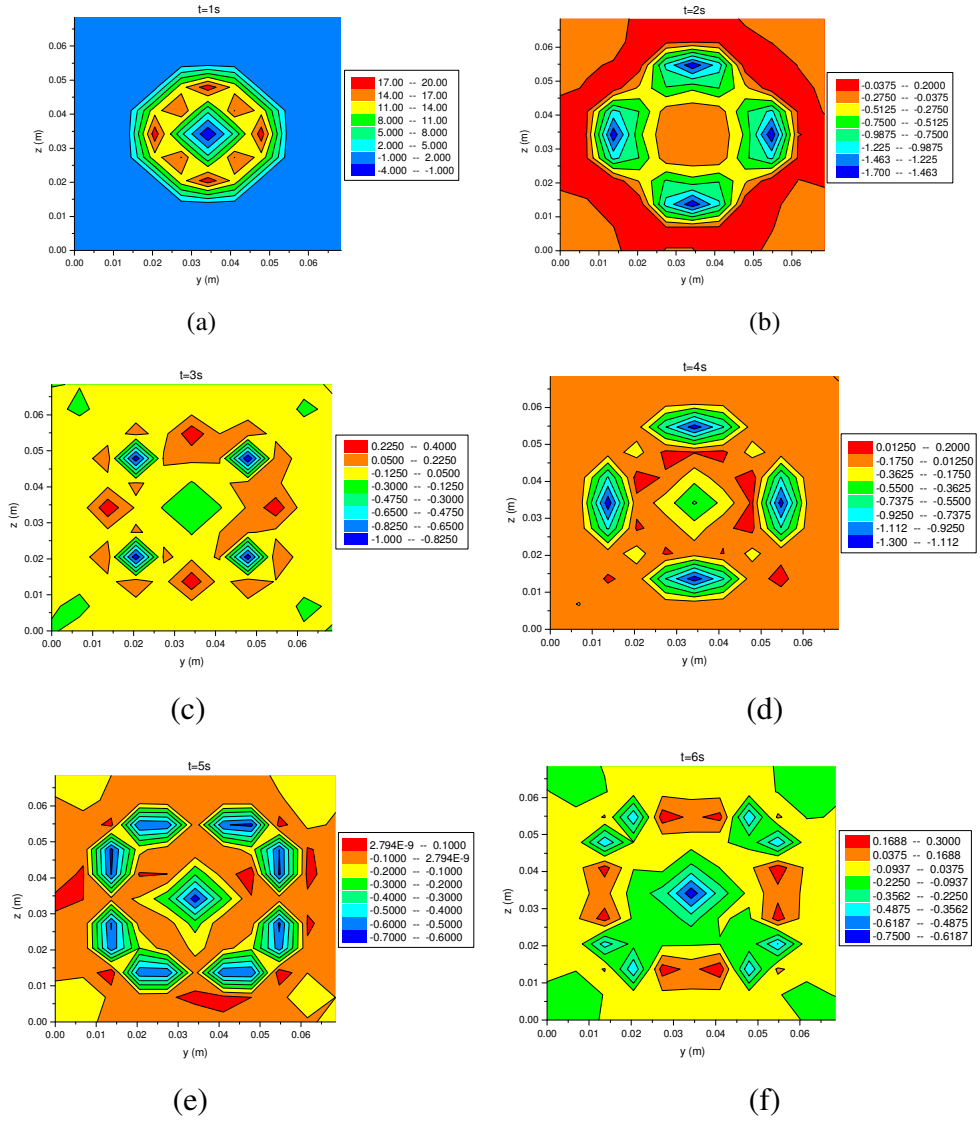

Figure 10 Contour distributions of the recovered temperatures errors (K) on the front surface at six times: (a) t = 1s; (b) t = 2 s; (c) t = 3 s; (d) t = 4 s. (e) t = 5s; (f) t = 6s.

The inverse solutions for $q_0^{"}$ is increased to 300 W/cm^2. are presented in Figs.11 (c)-(f). Figs. 11 (c) and 11 (d) show the recovered temperatures and the difference between the exact solution and recovered solution on the front surface at laser spot center. Comparing Fig. 11(d) and Fig.8 (b), we can see that the higher the heating flux ($q_0^{"}$), the larger the inverse error at the most drastic moment of pyrolysis. Figures 11 (e) and 11 (f) show the recovered temperatures and the difference between the exact solution and recovered solution at r = 13.4mm. The RMS error in the front-surface temperature is 7.69 K.

If the frequency of the front heating flux is high, it usually becomes more difficult to recover the periodic information (amplitude and phase) in the front-surface temperature based on the measurement data below the heating surface due to the damping and lagging effects of heat diffusion,. The effect of the frequency f on the inverse solutions is examined in Fig. 12, which shows the recovered temperatures at the laser spot center (r = 0) and at the radius of 13.4 mm for f = 5 Hz and $q_0^{"}$ = 150 W/cm^2. It can be seen that the temperatures at these two points can be well recovered. The RMS error in the front-surface temperature is 5.29 K.

CONCLUSIONS

A new numerical model is developed to simulate the 3-D inverse heat transfer in a composite target with pyrolysis and outgassing effects. The gas flow channel size and gas addition velocity are determined by using the rate equation of decomposition chemical reaction. In the 1-D compressible gas flow model, the gas addition in a laser-irradiated composite

Copyright © 2011 by ASME

material is accounted for with extra cross-sectional area in gas channel. The new gas flow model is incorporated into the 3-D direct and inverse heat conduction model. The evolvement of the gas channel shape and the distribution of the convective heat transfer coefficient are presented. Carbon/epoxy composite heated by high energy laser is taken as the demonstrative material. A nonlinear conjugate gradient method based on finite difference approach is employed for the numerical analysis.

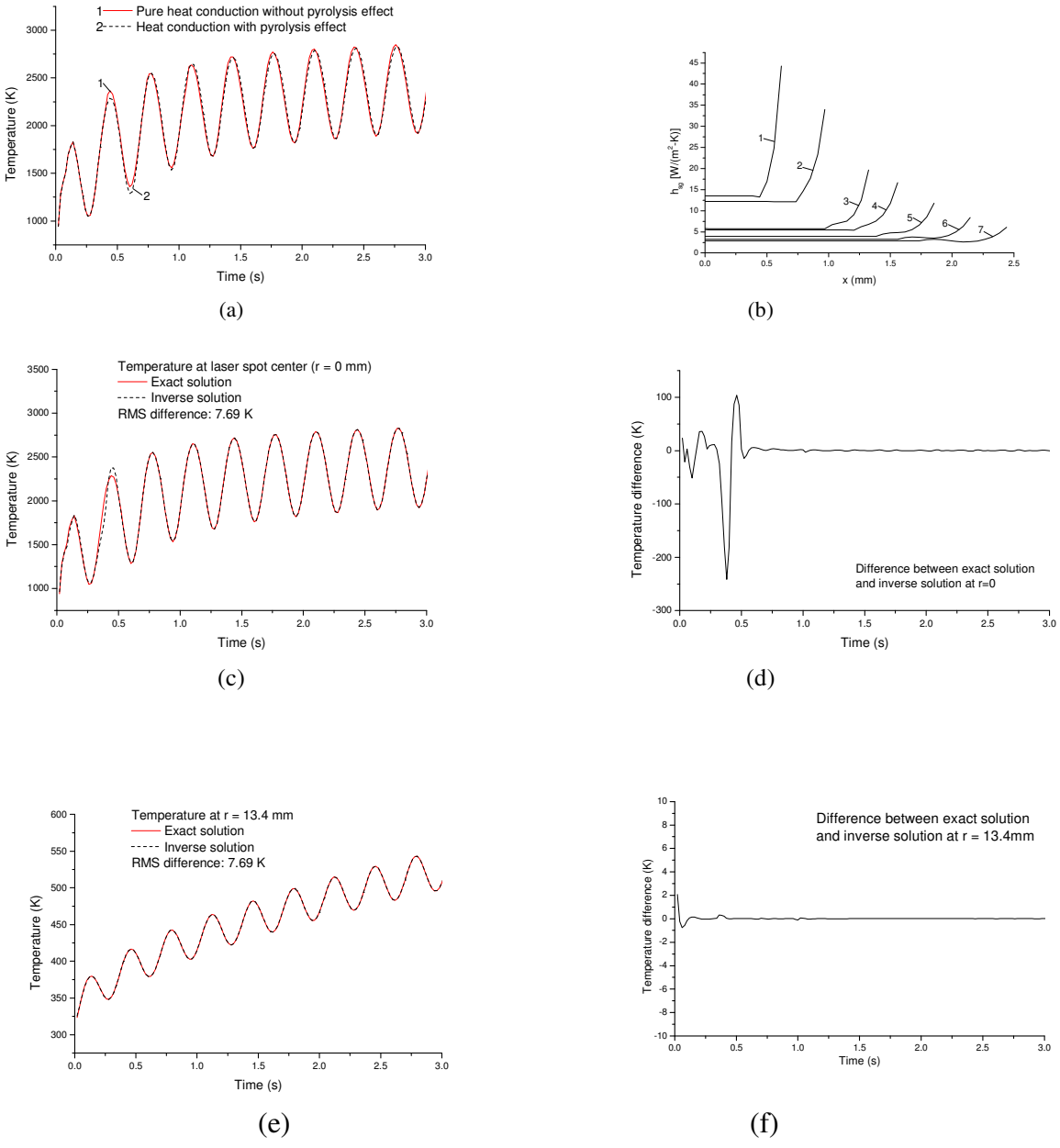

Figure 11 Calculating results for $q_0^{''}$ = 300 W/cm^2. (a) Cooling effect of pyrolysis gas flow; (b) Convective heat transfer coefficient along the x direction at different times, label is time (s); (c) comparison of exact solution and inverse solution at the laser spot center; (d) difference between the exact solution and inverse solution at the laser spot center (inverse solution minus exact solution); (e) comparison of exact solution and inverse solution at the radius of 13.4 mm; (f) difference between the exact solution and inverse solution at the radius of 13.4 mm (inverse solution minus exact solution).

Copyright © 2011 by ASME

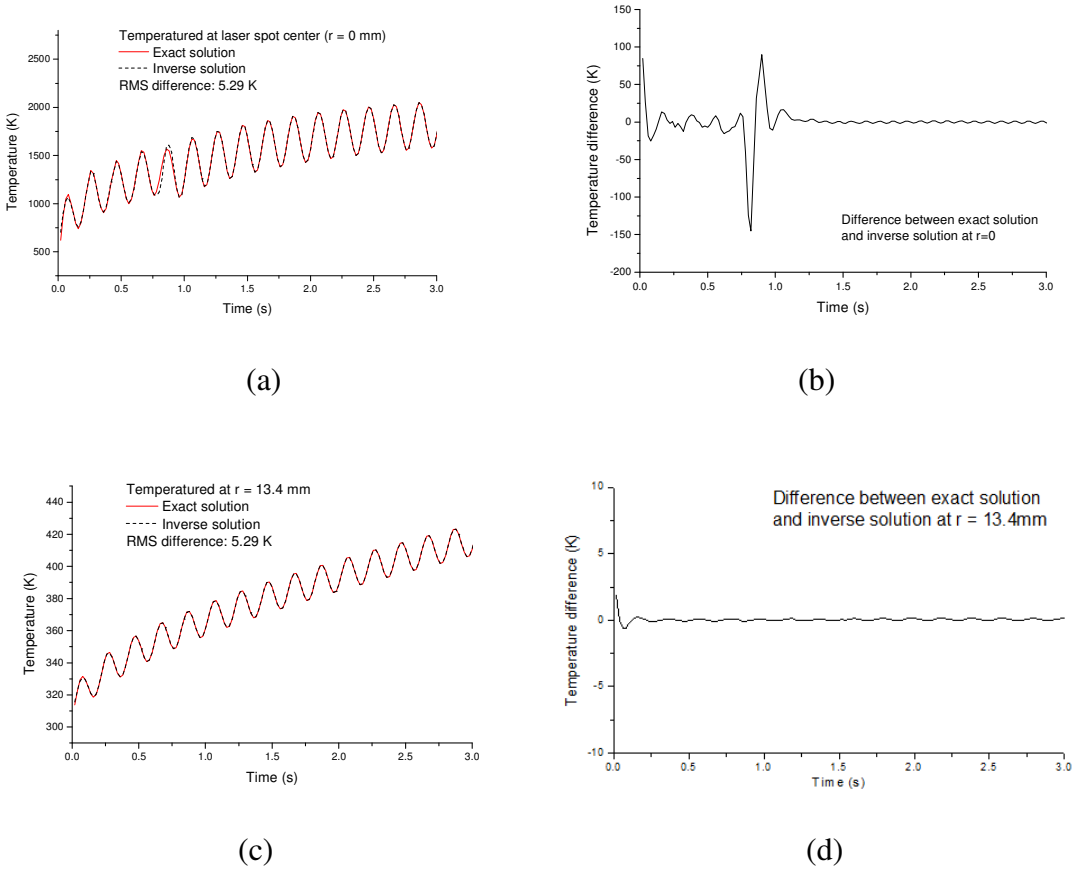

Figure 12 Recovered front surface temperature for f = 5 Hz. (a) comparison of exact solution and inverse solution at the laser spot center; (b) difference between the exact solution and inverse solution at the laser spot center (inverse solution minus exact solution); (c) comparison of exact solution and inverse solution at the radius of 13.4 mm; (d) difference between the exact solution and inverse solution at the radius of 13.4 mm (inverse solution minus exact solution).

It is found that increasing the laser heating flux can speed up the pyrolysis process, but can only enhance the convective heat transfer of early stage. The results also show that, with the new gas model, the front-surface temperatures can be well re-constructed based on the heat flux and temperature measurements on the back surface and temperature measurement at an interior plane, in the case where the interior plane is very close to the front surface.

ACKNOWLEDGMENTS

The authors would like to thank the Test Resource Management Center (TRMC) Test and Evaluation/Science & Technology (T&E/S&T) Program for their support. This work is funded by the T&E/S&T Program through the U.S. Army Program Executive Office for Simulation, Training and Instrumentation's contract number W900KK-08-C-0002. The authors would also like to express their gratitude to Dr. James L. Griggs for his valuable discussions.

Any opinions, findings and conclusions or recommendations expressed in this material are those of the author(s) and do not necessarily reflect the views of the Test Resource Management Center (TRMC) Test and Evaluation/Science & Technology (T&E/S&T) Program and/or the Program Executive Office for Simulation, Training & Instrumentation (PEO STRI).

REFERENCES

[1] Agarwal, B. D., and Broutman, L. J., *Analysis and Performance of Fiber Composites*, 2nd ed., John Wiley and Sons, New York, 1990.

[2] Reed, H. E., and Rice, M. H., 1993, "Failure of Solid Rocket Engines due to Laser Radiation Exposure," Cubed Report No. SSS-DFR-93-14222.

[3] Chen, J. K., Perea, A., and Allahdadi, F. A., "A Study of Laser/Composite Material Interactions," Composites Science and Technology, Vol.54, pp.35-44, 1995.

Copyright © 2011 by ASME

[4] Zhou, J., Zhang, Y., and Chen, J. K., and Smith, D. E., "A non-equilibrium thermal model for rapid heating and pyrolysis of organic composites," ASME *Journal of Heat Transfer*, Vol. 130, pp. 064501, 2008.

[5] Zhou, J., Zhang, Y., and Chen, J. K., "Numerical Simulation of Compressible Gas Flow and Heat Transfer in a Microchannel Surrounded by Solid Media," *International Journal of Heat and Fluid Flow*, Vol. 28, No.6, pp. 1484-1491, 2007.

[6] dell'Erba, M., Galantucci, L. M., and Miglietta, S., "An Experimental Study on Laser Drilling and Cutting of Composite Materials for the Aerospace Industry Using Excimer and CO_2 Sources," *Composites Manufacturing*, Vol.3, No.1, pp.14-19, 1992.

[7] Beck, J. V., Blackwell, B., and St-Clair, C. R., *Inverse Heat Conduction: Ill Posed Problems*, Wiley, New York, 1985.

[8] Özisik, M. N., and Orlande, H. R. B., *Inverse Heat Transfer: Fundamentals and Applications*, Taylor & Francis, New York, 2000.

[9] Yang, C. -Y. , and Chen, C. –K., "The boundary estimation in two-dimensional inverse heat conduction problems," *Journal of Physics D: Applied Physics*, Vol. 29, pp. 333-339, 1996.

[10] Emery, A. F., Nenarokomov, A. V., and Fadale, T. D., "Uncertainties in parameter estimation: the optimal experimental design," *International Journal of Heat and Mass Transfer*, Vol. 43, pp. 3331-3339, 2000.

[11] Frankel, J. I., Osborne, G. E., and Taira, K., "Stabilization of ill-posed problems through thermal rate sensors," *AIAA Journal of Thermophysics and Heat Transfer*, Vol. 20, No. 2, pp. 238-246, 2006.

[12] Loulou, T., and Scott, E. P., "An inverse heat conduction problem with heat flux measurements," *International Journal for Numerical Methods in Engineering*, Vol. 67, pp. 1587-1616, 2006.

[13] Aviles-Ramos, C., Haji-Sheikh, A., and Beck, J. V., "Exact solution of heat conduction in composite materials and application to inverse problems," *ASME Journal of Heat Transfer*, Vol. 120, pp. 592-599, 1998.

[14] Zhou, J., Zhang, Y., Chen, J. K., and Feng, Z. C., "Inverse estimation of surface heating condition in a three-dimensional object using conjugate gradient method," *International Journal of Heat and Mass Transfer,* Vol. 53, No. 13-14, pp. 2643-2654, 2010.

[15] Anderson, J. D., *Modern Compressible Flow with Historical Perspective*, Third Edition, McGraw-Hill, New York, 2003.

[16] John, J. E., and Keith, T. G., *Gas Dynamics*, Third Edition, Pearson Prentice Hall, New Jersey, 2006.

[17] Smith, D. E., Zhang, Y., and Chen, J. K., *HELVAMP: Laser/Composite Interaction Research Project*, Final Technical Report Submitted to Air Force Research Laboratory/Ball Aerospace, July, 2006.

[18] Childs, P. R. N., "Advances in temperature measurement," *Advances in Heat Transfer*, Vol. 36, pp. 111-181, 2002.

Copyright © 2011 by ASME